Metastable modular metastructures for on-demand reconfiguration of band structures and nonreciprocal wave propagation

Z. Wu,[1,*] Y. Zheng,[1,2] and K. W. Wang[1]

[1]*Department of Mechanical Engineering, University of Michigan, Ann Arbor, Michigan 48109-21255, USA*

[2]*State Key Laboratory for Strength and Vibration of Mechanical Structures, Xi'an Jiaotong University, Xi'an 710049, People's Republic of China*

(Received 25 August 2017; published 8 February 2018)

We present an approach to achieve adaptable band structures and nonreciprocal wave propagation by exploring and exploiting the concept of metastable modular metastructures. Through studying the dynamics of wave propagation in a chain composed of finite metastable modules, we provide experimental and analytical results on nonreciprocal wave propagation and unveil the underlying mechanisms that facilitate such unidirectional energy transmission. In addition, we demonstrate that via transitioning among the numerous metastable states, the proposed metastructure is endowed with a large number of bandgap reconfiguration possibilities. As a result, we illustrate that unprecedented adaptable nonreciprocal wave propagation can be realized using the metastable modular metastructure. Overall, this research elucidates the rich dynamics attainable through the combinations of periodicity, nonlinearity, spatial asymmetry, and metastability and creates a class of adaptive structural and material systems capable of realizing tunable bandgaps and nonreciprocal wave transmissions.

DOI: 10.1103/PhysRevE.97.022209

I. INTRODUCTION

Reciprocity of wave propagation is a fundamental principle [1,2] that describes the symmetry of wave transmission between two points in space. If a wave can propagate from a source to a receiver, it is equally possible for the wave to travel in the opposite path, from the receiver to the source. Motivated by the concept of electrical diodes, directional flow of electrons in the presence of electric field, much research attention has been devoted to exploring the possibility of breaking the time-reversal symmetry and realizing one-way propagation in various energy forms [3–9]. Since linear structures alone cannot break the reciprocity in reflection-transmission if time reversal symmetry is preserved [10,11], considerable efforts have been devoted to realize nonreciprocal behavior in linear systems with additional symmetry breaking mechanisms that are able to actively modulate system characteristics. For instance, Fleury *et al.* presented an acoustic circulator based on angular-momentum biasing through a circulating fluid [12]; Swinteck *et al.* demonstrated bulk waves with unidirectional backscattering-immune topological states using superlattice with spatial and temporal modulation of the stiffness [13]; and Wang *et al.* proposed an all-optical optical diode via a "moving" photonic crystal to control the flow of light [14]. In parallel to advances in spatiotemporal modulated linear systems, another major path to achieve nonreciprocal wave propagation is through using nonlinear systems. Liang *et al.* coupled a nonlinear medium with a supperlattice and accomplished unidirectional acoustic wave propagation by exploiting second-harmonic generation (SHG) of the nonlinear medium together with frequency selectivity of the linear lattices [7]. Popa and Cummer characterized an active acoustic metamaterial coupled to a nonlinear electronic circuit and demonstrated an isolation factor of >10 dB [15]. Recently, studies on nonreciprocal waves in systems with bistable elements have also received attention [16,17] for their intriguing nonlinear behavior [18].

While many of these and other pioneering studies pivoted on the realization of unidirectional energy transmission are intriguing, investigations on systems capable of on-demand tuning of such nonreciprocal wave propagations that are beneficial in many applications [19,20] are still limited. Boechler *et al.* illustrated that taking advantage of the localized defect mode, tunable rectification could be achieved by adjusting the static load of a defected granular chain [21]. They demonstrated the one-way wave propagation phenomenon experimentally for selected frequencies below and close to the defect frequency. Chen and Wu presented a tunable topological insulator through both analysis and numerical experiments using a 2D phononic crystal [22]. They showed the existence of the topologically nontrivial bandgaps by actively inducing airflow and frequency ranges that exhibit one-way wave propagation can be tuned by varying airflow velocity as well as lattice geometry. However, once the static load [21] or air flow rate [22] is fixed, both studies showcased the nonreciprocal harmonic wave propagations only for a limited frequency range. For transition waves, Raney *et al.* realized a tunable soft mechanical diode capable of one-way solitary wave propagation in elastomeric bistable lattices [23]. They observed unidirectional pulse propagation using a heterogeneous chain composed of a region with soft connectors combined in series with a region with stiff connectors and discovered that the propagation speed can be tuned by varying the beam end-to-end distance. While all these studies [21–23] demonstrate tunable nonreciprocal wave propagation, such adaptation can only be induced by the change of global

*wuzhen@umich.edu

topology or constraint. The reconfiguring of the numerous internal modules/components individually and synergistically for a given global confinement, which can significantly expand the adaptation space and greatly benefit wave control, are not allowed with the current approaches.

To advance the state of the art, in contrast to the previous methods, in this research we present an approach to accomplish nonreciprocal wave propagation for a broad frequency range with large adaptation space by exploiting the concept of metastable modular metastructures. These systems are composed of modules that individually exhibit *metastability*, i.e., coexisting of multiple internal stable states for the same topology, which cannot be achieved via pure bistable modules or modular systems explored in the past [16,17,21–23]. The assembled metasturctures are shown to exhibit direct pathways to facilitate synergistic property adaptation and bandgap tuning by harnessing the metastability and modularity, which are essential to creating the large adaptation space for nonreciprocal wave propagation. Hence, it is with such unique metastable composition and the integrated metastructure concept, we demonstrate that broadband nonreciprocal wave propagation and adaptation can be achieved.

To examine how the combination of nonlinearity, spatial asymmetry, periodicity, and metastability gives rise to unprecedented adaptive unidirectional wave propagation characteristics, the paper is organized as follows. In Sec. II, the overall concept of the proposed unit module and metastructure is introduced. In Sec. III, equations describing the nonlinear dynamics of the corresponding lattice chain are presented, followed by dispersion analysis of the corresponding linearized system. In Sec. IV, we present experimental evidence and analysis results of nonreciprocal wave propagation for the proposed architecture, discuss in detail the underlying mechanisms to realize nonreciprocal wave propagation, and demonstrate adaptivity of such anomalous transmission afforded via metastability.

II. OVERALL CONCEPT AND EXAMPLE METASTRUCTURE

The building block of the metastructure considered in this study is a metastable module consisting of a bistable spring and linear spring integrated in series [24,25]. With such arrangement, the proposed module will exhibit *metastability* that is essential to realize the broadband non-reciprocal wave propagation and adaptation. A lab test stand is set up to explore the concept. The bistable constituent is generated by press fitting three magnets with repulsive polarization inside a 3D printed enclosure connected in parallel with a stabilizing spring realized via spring steel. Characteristic force-displacement profile of a bistable element is measured with an Instron machine, shown in Fig. 1(a). The bistable element is then connected in series with a linear spring steel to form a metastable module. A characteristic force-displacement profile of the module is depicted in Fig. 1(b). As shown in Fig. 1(b), the building block exhibits a metastable range, where two metastable states (internal configurations) coexist with the same overall topology (global displacement). The experimental setup of the metastructure consists of a chain of such metastable modules connected in series horizontally, aligned with guiding rail and linear sliding bearings. Figure 1(c) depicts the top view of the experimental test bed and Fig. 1(d) shows the corresponding schematic of the metastructure in which the bistable constituents are represented with buckled beams, the linear constituents are represented with coil springs and the inertial elements are symbolized with orange and yellow circles. As denoted in Fig. 1(d), free length of the structure L_{free} is defined to be the zero force position when all the bistable elements are buckled to the left and the global displacement z is defined as the additional deformation applied to the structure starting from the free length L_{free} position. In this research, we focus on steady-state wave propagation through the metastructure as the chain is harmonically driven from one end. To investigate the nonreciprocal effect, two actuation scenarios are considered: one is forward actuation with actuator on the left side of the lattice chain and the other is backward actuation with actuator on the right-hand side of the chain. The conceptual representation of the excitation scenarios is depicted in Fig. 1(e). For illustration purposes, only inertial elements denoted by orange and yellow circles are presented in Fig. 1(e), while the stiffness constituents connecting the masses are not shown. For both scenarios, harmonic displacement input x_{in} is directly applied to the mass next to the boundary of the chain indicated by square, and output signal x_{out} is measured one module away from the boundary marked with circle, Figs. 1(c) and 1(e). During the experiments, both input and output displacements are measured with laser vibrometers.

III. MATHEMATICAL MODEL AND BAND STRUCTURE ANALYSIS

A. Metastable states

Figure 2 depicts a 1D discrete lattice representation of N identical metastable modules connected in series. Each metastable module, highlighted with red dashed box, consists of two masses m_1 and m_2 coupled via a linear constituent; the modules are interconnected by bistable springs. Without loss of generality, the bistable and linear restoring forces are assumed of the form, $F_{NL} = -k_1 x + k_3 x^3$ and $F_L = k_L y$, where x and y are the deformations of bistable and linear springs, respectively. The total potential energy of the metastable chain for a fixed global displacement z measured from its free length L_{free} can be expressed as

$$U = \sum_{i=1}^{N-1}\left[\frac{k_L}{2}(x_{[i]2} - x_{[i]1})^2 - \frac{k_1}{2}(x_{[i+1]1} - x_{[i]2})^2 + \frac{k_3}{4}(x_{[i+1]1} - x_{[i]2})^4\right] + \frac{k_L}{2}(z - x_{[N]1})^2 - \frac{k_1}{2}x_{[1]1}^2 + \frac{k_3}{4}x_{[1]1}^4, \tag{1}$$

which is a function of internal mass displacements $x_{[i]1}$, $x_{[i]2}$, where subscript i refers to the ith module. All internal displacements $x_{[i]1}$ and $x_{[i]2}$ are measured from the individual positions of the free length configuration. For a fixed global displacement z, equilibrium positions of metastructure satisfy $\partial U/\partial x_{[i]1} = 0$ and $\partial U/\partial x_{[i]2} = 0$ under the constraint that $\sum_{i=1}^{N-1}(x_{[i]1} + x_{[i]2}) + x_{[N]1} = z$. According to the minimum potential energy principle [26,27], metastable states of the

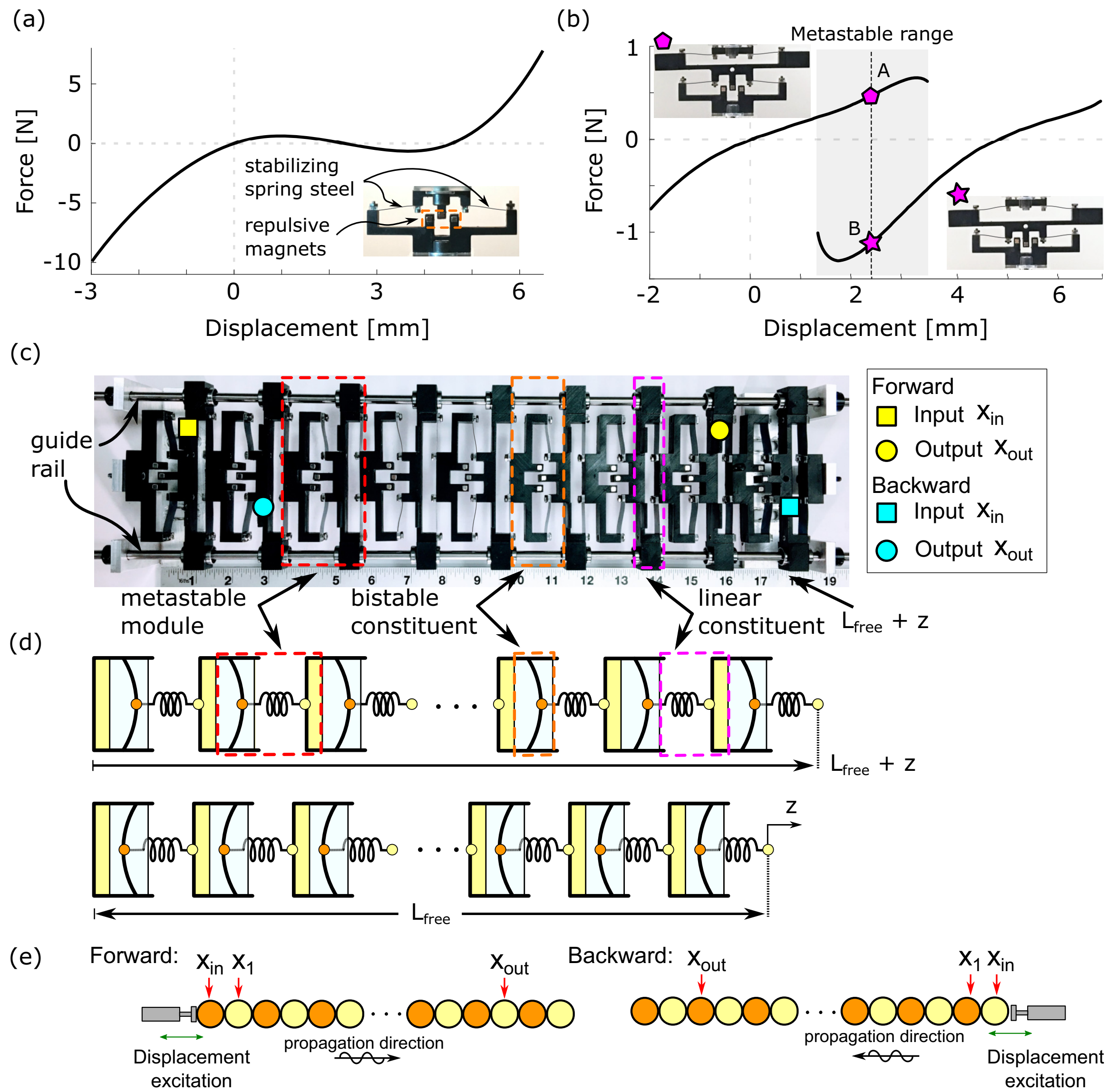

FIG. 1. (a) Characteristic force displacement profile of a bistable element. (b) Characteristic force displacement profile of a metastable module. (c, d) Top view and corresponding schematic of the experiment setup. (e) Conceptual diagrams of metastable module assembled in series under forward (excitation from left) and backward (excitation from right) actuations.

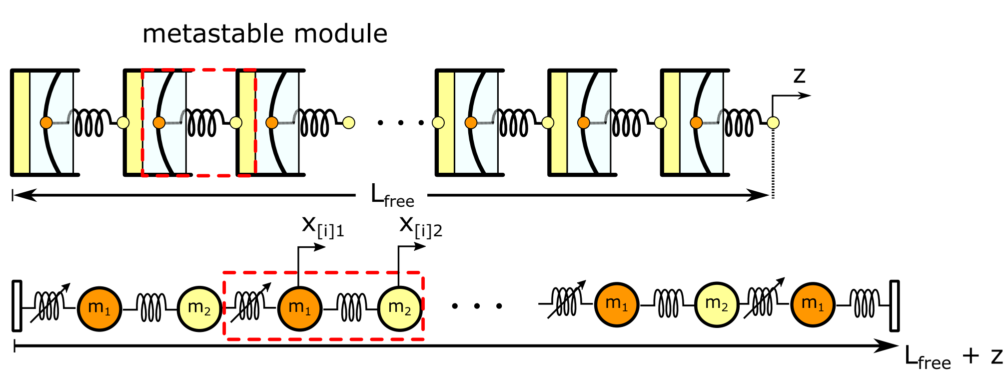

FIG. 2. Schematic and discrete mass spring representation of an N metastable module assembled in series. A periodic unit cell, in this case same as the metastable module, is highlighted with red dashed box.

chain satisfy $\partial^2 U/\partial x_{[i]k}\partial x_{[j]l} > 0$, i.e., the Hessian matrix of the potential is positive definite.

B. Governing equations and linear dispersion analysis

In general, for a fixed global displacement z, a chain of N metastable modules can have up to 2^N metastable states (internal configurations) with varying system properties [24,25]. Starting from one of the metastable states, equations of motion for the ith module, can be expressed as

$$m_1\ddot{x}_{[i]1} + F_{NL}(x_{[i]1} - x_{[i-1]2}) + k_L(x_{[i]1} - x_{[i]2}) = 0, \quad (2a)$$

$$m_2\ddot{x}_{[i]2} + F_{NL}(x_{[i]2} - x_{[i+1]1}) + k_L(x_{[i]2} - x_{[i]1}) = 0. \quad (2b)$$

Equation (2a) is applicable to $\forall i = 2$ to N and Eq. (2b) is applicable to $\forall i = 1$ to N-1. Due to the fixed boundary conditions, equations of motion for first and last mass in the chain can be modified as

$$m_1\ddot{x}_{[1]1} + F_{NL}(x_{[1]1}) + k_L(x_{[1]1} - x_{[1]2}) = 0 \quad (3a)$$

$$m_1\ddot{x}_{[N]1} + F_{NL}(x_{[N]1} - x_{[N-1]2}) + k_L(x_{[N]1} - z) = 0 \quad (3b)$$

Depending on the excitation scenarios, Fig. 1(c), external excitation will be directly applied to the first or last mass in the chain.

To establish a linear dispersion relation, we first linearize the equations of motion about its metastable state and the band structure is determined by modeling a repeating periodic unit cell of an unforced, infinite chain. For the diatomic chain depicted in Fig. 2, the periodic unit cell is the same as a metastable module, and the linearized equation can be written as

$$m_1\ddot{\zeta}_i + \tilde{k}_{NL}(\zeta_i - \eta_{i-1}) + k_L(\zeta_i - \eta_i) = 0 \quad (4a)$$

$$m_2\ddot{\eta}_i + \tilde{k}_{NL}(\eta_i - \zeta_{i+1}) + k_L(\eta_i - \zeta_i) = 0 \quad (4b)$$

where ζ_i and η_i are small perturbation of mass m_1 and m_2 around its initial positions and $\tilde{k}_{NL}$ is the corresponding linearized stiffness of the bistable spring. Assuming solutions in the form of a traveling wave, i.e., $\zeta_i = A\exp[j(\omega t - kiL)]$ and $\eta_i = B\exp[j(\omega t - k(i+1)L)]$, where k is the wave number and L is unit length, the model is reduced to a standard eigenvalue problem:

$$\begin{bmatrix} \frac{k_L+\tilde{k}_{NL}}{m_1} & -\frac{\tilde{k}_{NL}+k_L e^{-jkL}}{m_1} \\ -\frac{\tilde{k}_{NL}+k_L e^{jkL}}{m_2} & \frac{k_L+\tilde{k}_{NL}}{m_2} \end{bmatrix}\begin{bmatrix} A \\ B \end{bmatrix} = \omega^2\begin{bmatrix} A \\ B \end{bmatrix} \quad (5)$$

The band structure can then be determined by sweeping the wave number k from 0/L to $\frac{\pi}{L}$. In general, due to the existence of multiple metastable states for a chain of N metastable modules, depending on the initial configuration, periodic repeating cell should be identified, and similar dispersion analysis can be carried out accordingly.

C. Analysis results of band structures

For exploration purposes and without loss of generality, parameters used in the analysis are chosen to be of arbitrary unit. With stiffness $k_1 = 1$, $k_3 = 1$, $k_L = 0.2$ and masses $m_1 = m_2 = 1$, Fig. 3(a) depicts the resultant force profile of the metastructure as global displacement changes. Due to a synergistic product of assembling together metastable modules, multiplying number of different internal configurations can be afforded via transitioning among these metastable states for

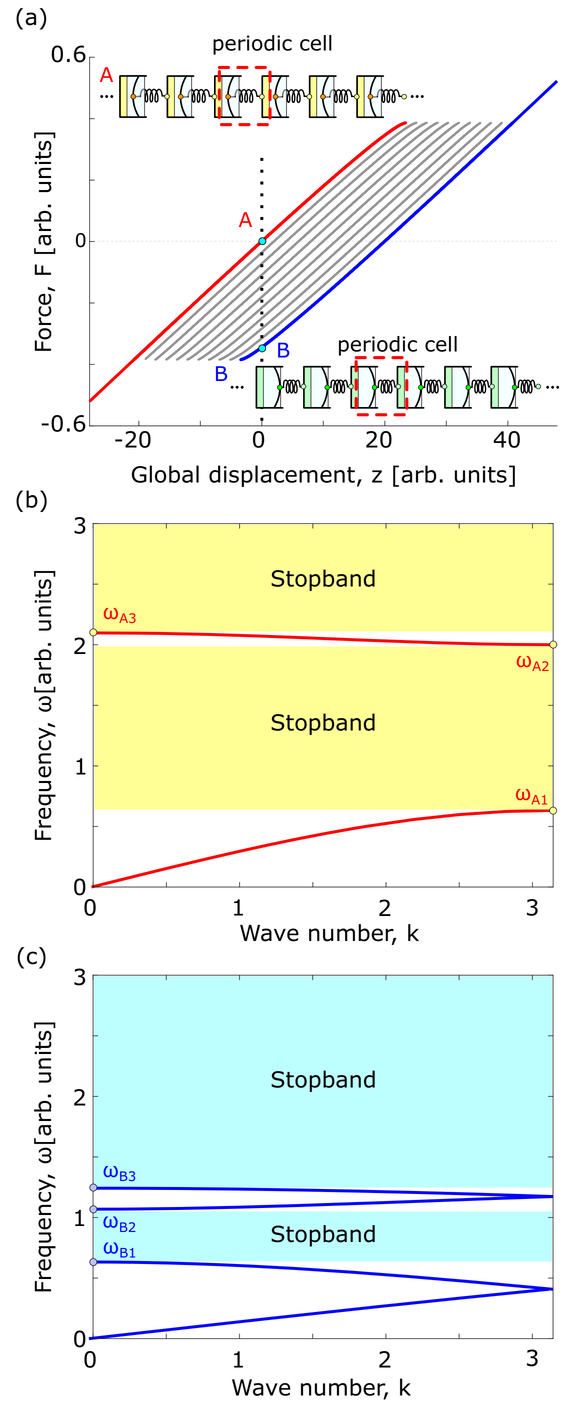

FIG. 3. (a) Reaction force profile as a function global displacement for a 10 module metastable chain. Points A, B are two different configurations for the same global topology realized by internal configuration switching. (b, c) Corresponding band structures for configurations A and B. Passband are within [0, ω_{A1}], [ω_{A2}, ω_{A3}] and [0, ω_{B1}], [ω_{B2}, ω_{B3}], respectively, demonstrating the massive band structures tunability via internal configuration switching.

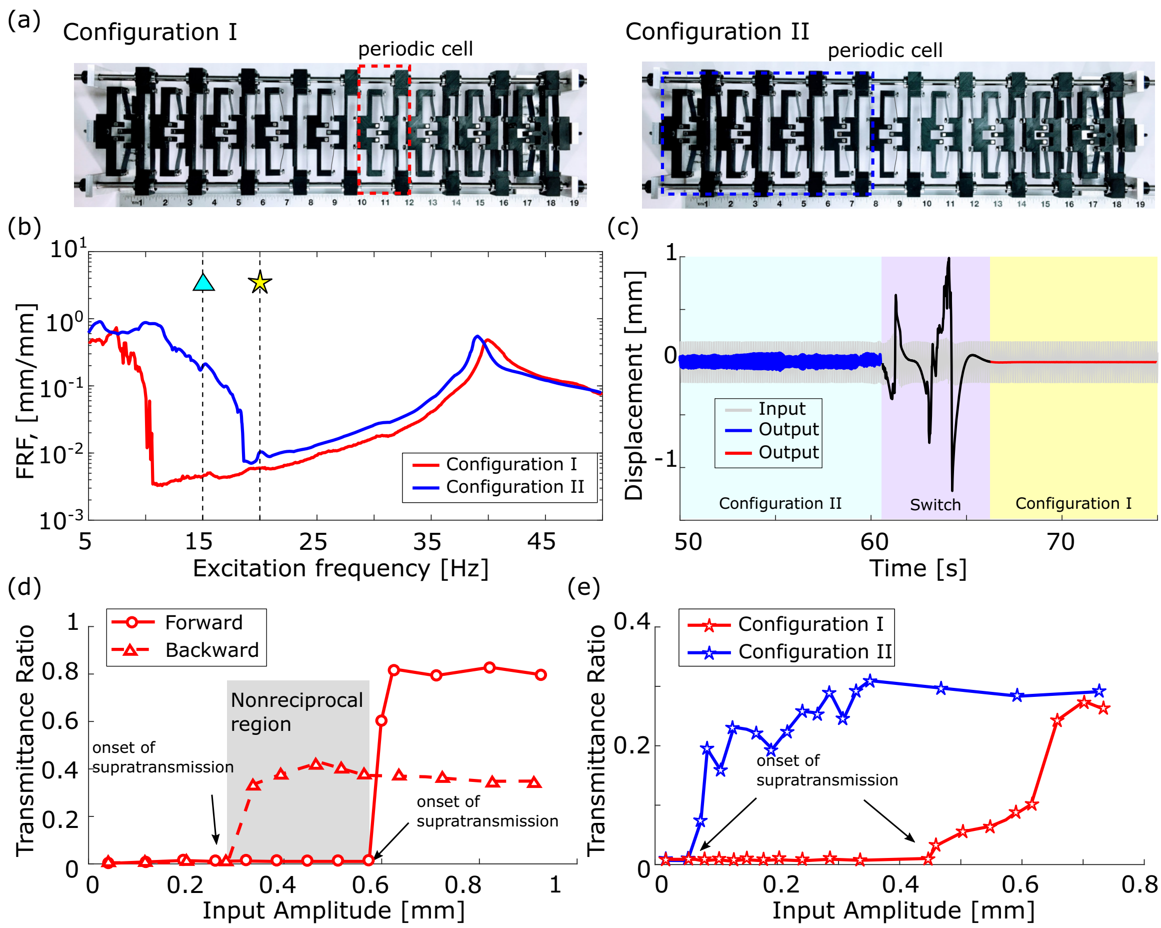

FIG. 4. (a) Top view of experiment setup with two different configurations. Two configurations can be reconfigured by switching between metastable states. Periodic cell of each configuration is highlighted with dashed box. (b) FRF of output displacement over input displacement as input excitation frequency changes for configuration I (red) and configuration II (blue) with small excitation level. Frequency 15 Hz (triangle) is in the passband for configuration II and stopband for configuration I and 20 Hz (star) is in the stopband for both configurations. (c) Time history of output displacement with input RMS displacement 0.2 mm and input frequency at 15 Hz. Signal changes *in situ* from propagating to nonpropagating as configuration changes from configuration II to I. (d) Transmittance ratio (TR) for forward (circles connected with solid line) and backward (triangles connected with dashed line) actuation for configuration I with input frequency at 15 Hz. Shaded area denotes the region of nonreciprocal wave propagation. (e) Transmittance ratio (TR) for configurations I and II under forward actuation at 20 Hz (circles connected with solid lines), demonstrating the adaptiveness of supratransmission.

the same global displacement z [24,25]. Since each metastable state exhibits unique system property [24,25], the ability to reconfigure among these states exemplifies the broad adaptation space of the proposed metastructure for wave propagation. For instance, configurations A and B in Fig. 3(a) represent two possible periodic chains of the same global length with different internal configurations or metastable states. Periodic unit cells for the two configurations are highlighted with red dashed box in Fig. 3(a) and the corresponding band structures for configurations A and B are depicted in Figs. 3(b) and 3(c), respectively. For both configurations A and B, the periodic cells consist of a single metastable module with different internal configurations, Fig. 3(a). As illustrated in Fig. 3, property programmability can be realized via metastable state switching, demonstrated by the adaptation of band structures of the metastable chain. For configuration A, the two passbands are [0, 0.633] and [2, 2.098], whereas for configuration B, the first passband remains to be the same [0, 0.633], while the second passband shifts to [1.069, 1.242].

IV. NONRECIPROCAL WAVE PROPAGATION AND ADAPTATION

A. Experimental investigation

With the same global confinement of 45.1 cm (17.75 inches), two configurations I and II of the experiment setup are depicted in Fig. 4(a). The two configurations are obtained by switching between metastable states and the periodic repeating cells are highlighted with dashed boxes. To first identify the band structures, frequency sweep tests are performed for both configurations with input RMS acceleration $0.3\,m/s^2$ via an electromagnetic shaker. Due to limitation of the shaker, the frequency range is selected to be from 5 to 50 Hz and the sweep rate is chosen to be 0.05 Hz/s. Figure 4(b) depicts the displacement frequency response function (FRF) in forward actuation direction, with blue and red representing configurations I and II, respectively. As depicted in Fig. 4(b), the first passband for configuration I extends to approximately 10 Hz and for configuration II, the first passband ends at around 18.5 Hz. Therefore, for excitation frequency in between 10 and 18.5 Hz, wave propagation characteristics can be adaptively tuned between propagating and nonpropagating, as the proposed structure reconfigures between metastable states I and II. Furthermore, such adaptation can be exploited *in situ*, depicted by the displacement time history in Fig. 4(c). With input RMS displacement 0.2 mm and input frequency 15 Hz (gray), the system starts in configuration II and at steady state the vibration energy is able to propagate through the chain since the excitation frequency is inside the passband (blue). We then switch to configuration I manually by sequentially reconfiguring two bistable constituents, while the metastructure is still harmonically excited, depicted by the consecutive spikes in time history (black) in Fig. 4(c). After switching *in situ* to configuration I, the excitation frequency changes from inside the passband to stopband, and as a result, the output displacement is reduced significantly to nearly zero (red). Therefore, due to band structure adaptation, we are able to *in situ* create immediate change of wave propagation characteristics as system reconfigures.

To illustrate the nonreciprocal wave propagation phenomenon, metastructure is prescribed in configuration I and is excited at 15 Hz. The excitation frequency is chosen such that it is inside the stopband of the linearized structure. With the same starting configuration, system is excited in forward and backward actuation scenarios individually with a fixed input amplitude and the corresponding output and input displacements are measured using laser vibrometers. The same experimental procedures are then repeated for different input excitation amplitudes. Figure 4(d) summarizes the results of transmittance ratio for different input amplitudes and the discrete points circle (triangle) for forward (backward) excitation scenarios are connected with solid (dashed) lines to illustrate the trend. The transmittance ratio (TR) is defined as the ratio of steady-state output RMS displacement over input RMS displacement $\mathrm{TR} = \frac{|\bar{x}_{\mathrm{out}}|}{|\bar{x}_{\mathrm{in}}|}$. As indicated in Fig. 4(d), with small excitation level, due to the bandgap effect, the output displacement is negligible compared to the input amplitude for both excitation directions. As input amplitude increases to 0.3 mm, transmittance ratio of the backward actuation increases significantly, while it remains to be low for forward actuation, depicted in Fig. 4(d), providing experimental evidence on the start of nonreciprocal wave propagation. This unidirectional energy transmission phenomenon ends at input amplitude 0.58 mm, at which sudden increase in the output amplitude for the forward actuation is also made possible. Such amplitude-dependent wave transmission feature corroborates with studies on supratransmission, in which energy of a signal with input frequency in the stopband is able to transmit through a nonlinear chain when input amplitude exceeds certain threshold [28–33]. For the proposed architecture, integrating the supratransmission property of a nonlinear periodic chain with spatial asymmetry, the metastable structure is capable of attaining the onset of supratransmission at different input amplitude levels depending on actuation direction, and this threshold discrepancy creates a region that facilitates the nonreciprocal wave propagation.

In addition to nonreciprocal wave propagation, endowed with metastability, the proposed structure is also capable of exhibiting onset of supratransmission at different excitation level by internal reconfiguration. As illustrated in Fig. 4(e), the metastructure is excited under forward actuation at 20 Hz for both configurations I and II. Similar to previous studies, structures are excited with fixed input amplitude for each configuration and these individual tests are connected with lines to illustrate the trend on wave propagation characteristics as input amplitude increases. Since under small excitation level, the metastructure resembles that of a linear system and energy does not transmit through the chain given that the input frequency is within the stopband for both configurations. As input amplitude increases to 0.06 mm, energy starts to transmit through the chain for configuration II, whereas wave propagation is still prohibited for configuration I until excitation level reaches 0.45 mm, after which wave propagates through the chain for both configurations. Such adaptivity on the onset of supratransmission for different configurations is crucial to create systems with on-demand tuning of nonreciprocal wave propagation characteristics.

B. Analysis results–Generation of nonreciprocal wave propagation

To understand the mechanisms of nonreciprocal wave propagation of the proposed system, a detailed numerical analysis is performed using the same system parameters for dispersion analysis discussed in Sec. 3.3. Wave propagation characteristics are first explored for configuration A, defined in Fig. 3, under both forward and backward actuations. Small damping coefficients $\zeta = \frac{c}{\sqrt{k_1 m_1}} = 0.001$ is applied between lattices and simulations are performed for sufficiently long time ($30\,000\omega_1$ where ω_1 is defined as $\sqrt{\frac{k_1}{m_1}}$) to reach steady state. Small damping coefficients are chosen to limit the influence of energy dissipation on the transmission reduction phenomenon. Figure 5 depicts the displacement time history and FFT of corresponding velocities for input x_{in} (magenta), output x_{out} (cyan) and response of internal mass adjacent to input x_1 (gray), Fig. 1(c). Driving frequency $\omega = 1.15$ is chosen to be within the attenuation band [0.633, 2] of the metastructure for configuration A from dispersion analysis and two input amplitudes $\delta = 0.1$ and 0.5 are considered.

For small input amplitude $\delta = 0.1$, despite the large discrepancy on steady-state amplitude of internal mass (gray) between backward and forward actuations, the output response amplitudes (cyan) are both negligible compared to that of the input (magenta), Figs. 5(a) and 5(c). Difference in response amplitudes of the internal masses is due to the inherent spatial asymmetry of the metastable chain introduced by modules with different elastic constituents. With finite lattice length, one end of the chain is grounded via a linear constituent, whereas the other end is fixed through a nonlinear constituent, Fig. 1. To understand the wave propagation characteristics, FFT of the corresponding velocities are depicted in Figs. 5(b) and 5(d). Red dashed lines are band structure boundaries ω_{A1}, ω_{A2}, and ω_{A3} determined from the linear analysis, Fig. 3(b). For both actuation scenarios, a majority of the energy is localized around the fundamental driving frequency ω_d as well as its higher harmonics $2\omega_d$ and $3\omega_d$, Figs. 5(b) and 5(d). In complement to the time domain analysis, the FFT results also reveal that response amplitude of the internal mass

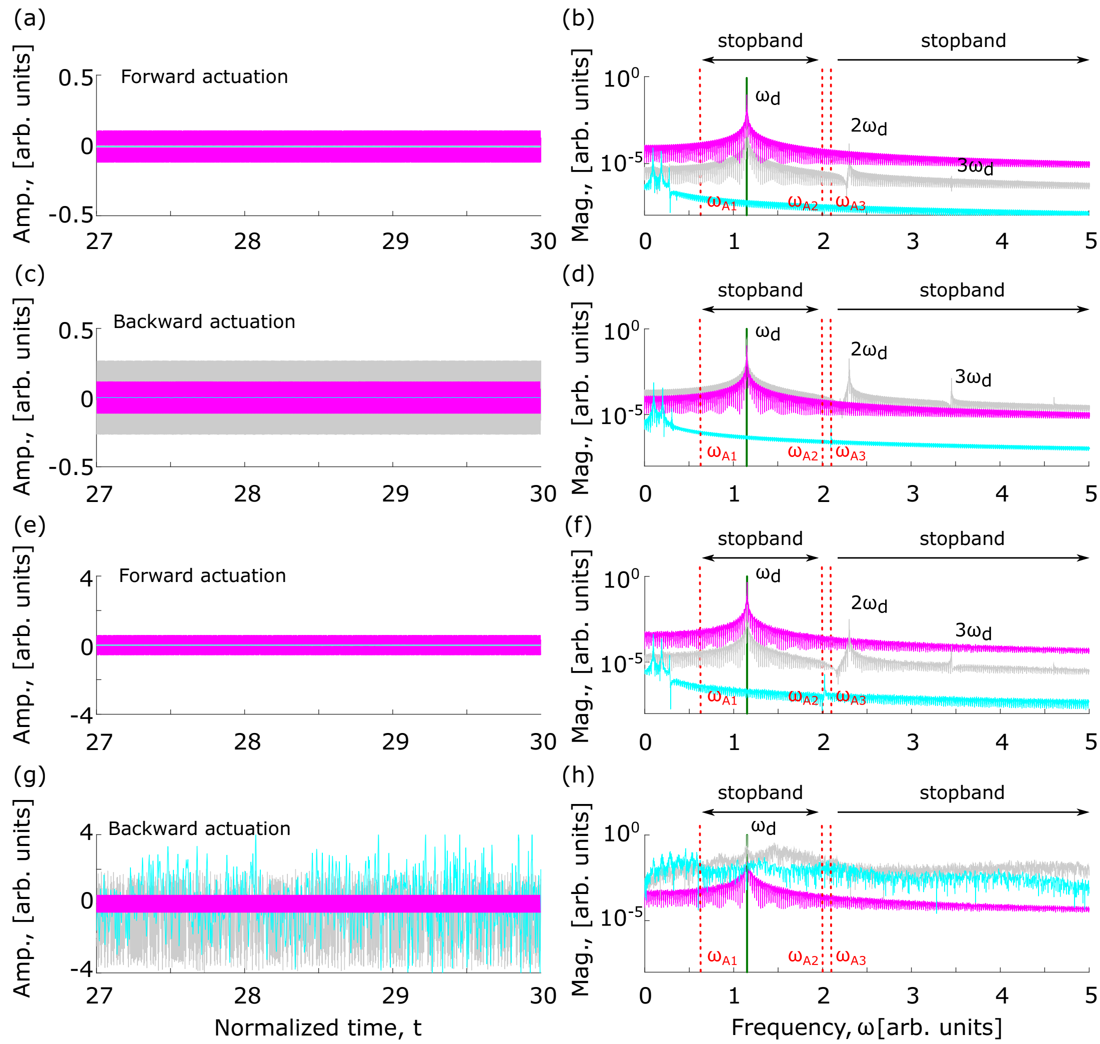

FIG. 5. Steady-state displacements of input (magenta), output (cyan), and internal (gray) masses for configuration A shown in Fig. 3 under forward [(a) and (e)] and backward [(c) and (g)] actuation with excitation frequency $\omega_d = 1.15$ and excitation amplitude $\delta = 0.1$ [(a) and (c)] and $\delta = 0.5$ [(e) and (g)]. (b, d, f, h) Frequency domain analysis of corresponding velocities. Red dashed lines are band structure boundaries frequencies for configuration A predicted from linear analysis and green solid line is the input driving frequency. Time t is normalized with respect to the natural frequency $\omega_1 = \sqrt{\frac{k_1}{m_1}}$.

for backward actuation is orders of magnitude greater than that for the case of forward actuation, due to the inherent spatial asymmetry. In fact, amplitude of the second harmonic $2\omega_d$ under backward actuation is still two times larger than the amplitude of fundamental harmonics ω_d under forward actuation. However, since these dominant frequencies reside within the stopband of the metastable lattices, majority of wave energy does not propagate through the metastable chain. As exemplified by the frequency response of output signal for both scenarios, dominant frequencies of the remaining wave energy are prominently localized inside the first passband. Yet, since the vibration amplitudes of the output signals are considerably reduced compared to that of the input, transmittance ratios are negligible.

As input amplitude increases to $x_{\text{in}} = 0.5$, wave propagation for forward excitation scenario is still largely prohibited, similar to the low amplitude actuation case, Figs. 5(e) and 5(f). However, comparing Figs. 5(e) and 5(g), the response of output signal increases substantially for backward actuation. More specifically, with large enough input amplitude, the subsequent internal masses (gray) instantly undergoes large amplitude vibration, in this case chaotic response, Fig. 5(g). Therefore, even though the driving frequency is within the nonpropagating zone, input frequency is immediately redistributed amongst a broad frequency range and wave energy is transmitted through the chain with frequencies spectrum primarily inside the propagating passband, Fig. 5(h). This frequency conversion property is a classical nonlinear phenomenon and substantiates previous researches in which supratransmission is enabled via nonlinear instability and the transmitted signal becomes quasiperiodic or chaotic [30–34]. Hence, we can conclude that non-reciprocal wave transmission with the proposed metastructure is facilitated through the interplay of spatial asymmetry, nonlinearity and periodicity. Use the same definition of transmittance ratio (TR), it is determined that with the given parameters, TR for forward and backward actuations are 0.01

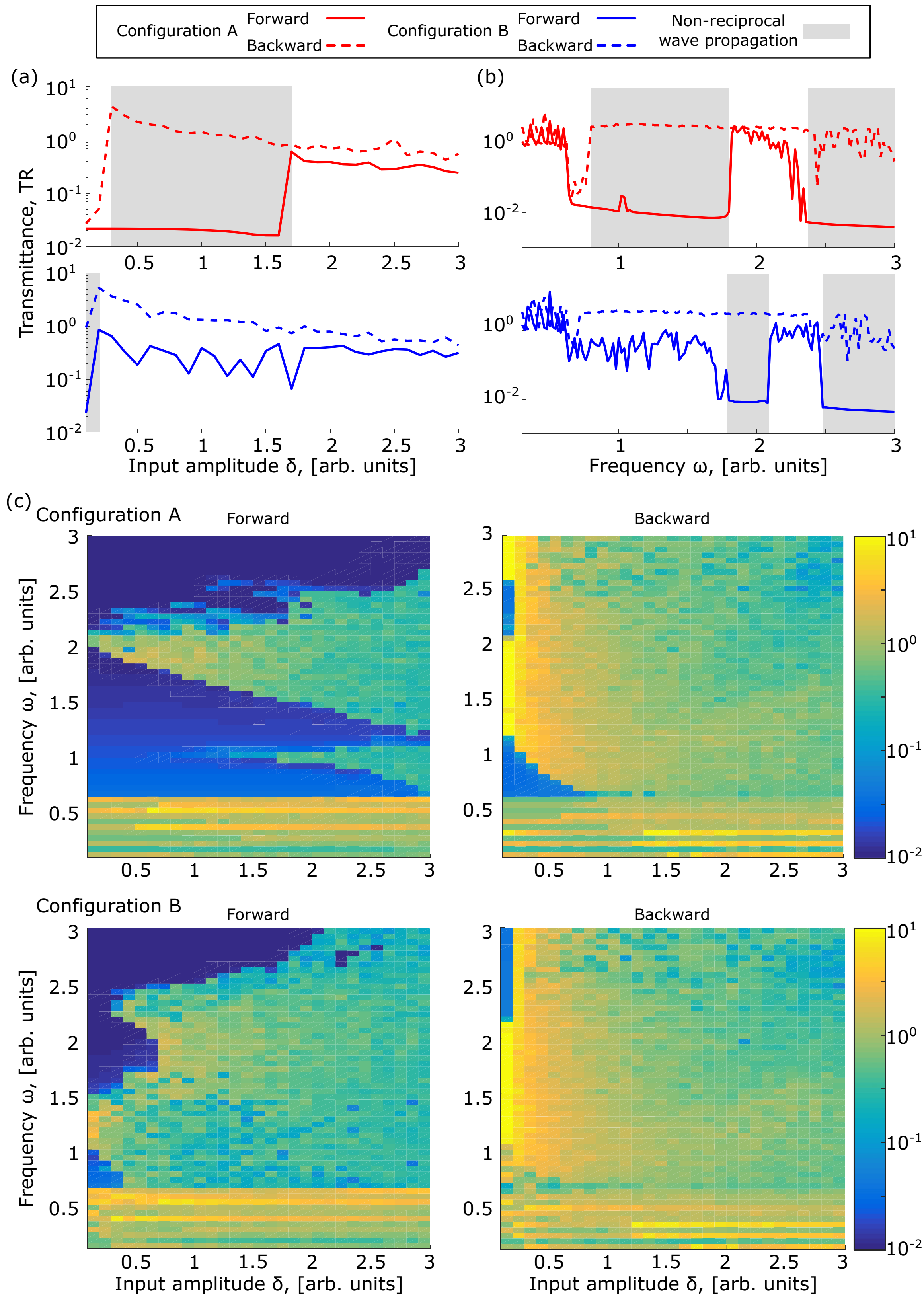

FIG. 6. (a, b) Transmittance ratio (TR) for metastructure under forward (solid line) and backward (dashed line) actuation for configuration A (red) and B (blue) with shaded areas denoting parameter space for nonreciprocal wave propagation. (a) Varying input amplitude with fixed frequency $\omega_d = 0.95$ and (b) Varying input frequency with fixed amplitude $\delta = 0.5$. Gray area indicates the region of nonreciprocal wave transmission. (c) Contour plot on transmittance ratio (vs. input frequency and amplitude) of forward and backward actuation for configurations A and B.

and 3.73, respectively, demonstrating more than two orders of magnitude increase in transmittance as excitation direction changes and providing clear evidence of nonreciprocal wave transmission.

C. Analysis results—Adaptive wave propagation

Experimental and numerical studies discussed in previous sections demonstrate the nonreciprocal wave transmission characteristics as input excitation amplitude varies. Experimental observations also indicate that such anomalous energy flow is not only a result of the nonlinearity and spatial asymmetry of metastructure, but also tightly related to the bandgaps of the periodic chain. To further investigate the influence of internal reconfiguration (change of metastable states) on the TR and nonreciprocity of the metastable lattice, numerical analysis is performed on the same metastructure by varying both internal configuration and actuation scenarios. Figure 6(a) depicts the transmittance ratio as input amplitude changes under constant input frequency $\omega = 0.95$. This frequency is within the stopband for both configurations A and B. Similar to experiment investigations, starting in each configuration, harmonic excitation with fixed input amplitude is applied to one end of the chain depending on the excitation scenarios.

For small input amplitude, configuration A (red lines), both forward and backward actuations have small transmittance ratio, similar to previous observations. Yet, due to spatial asymmetry, as input amplitude increases to 0.3 m, transmittance ratio for backward actuation increases significantly by two orders of magnitude, red dashed line, whereas TR for forward actuation remains to be low, indicating the start of nonreciprocal wave transmission. Same as the experimental observation in Fig. 4(d), backward actuation is able to trigger the onset of supratransmission with smaller excitation amplitude than forward actuation.

As input amplitude increases to 1.7, input energy is sufficient to trigger large amplitude vibration for forward actuation and is reflected by the large increase in transmission ratio, red solid line. Further increasing input amplitude beyond 1.7, wave energy will transmit in both directions. Hence, for configuration A, nonreciprocal wave transmission occurs for input amplitudes between 0.3 to 1.7. As the metastructure is changed to configuration B [bottom row in Fig. 6(a)] by switching between the metastable states [Fig. 3(a)], with the same excitation frequency $\omega = 0.95$, amplitude range for such unidirectional energy transmission now shifts to between 0.1 to 0.2. This is due to the fact that comparing with configuration A, configuration B corresponds to a softer state, i.e., equilibrium position is at a shallower potential well, evidenced by a lower passband, Fig. 3(b). Therefore, nonlinear instability is more readily attainable compared to configuration A. This demonstrates the adaptivity of nonreciprocal wave transmission characteristics as switching amongst the metastable states.

Additionally, as shown in Fig. 3, alternating internal configurations can greatly affect the bandgaps of the metastable lattice, which is shown to be pivotal in manipulating frequency spectrum of the output signal, Fig. 5. Hence, the effect of input frequency on the nonreciprocal wave transmission characteristics as switching amongst metastable states is investigated. Figure 6(b) illustrates the transmittance ratio as input frequency changes with constant input amplitude $\delta = 0.5$. It can be seen that for configuration A, nonreciprocal transmission exists for frequencies between [0.7, 1.7] and [2.3, 3] and is changed to [1.7, 2] and [2.5, 3] as switched to configuration B.

To further explore the adaptivity of wave propagation characteristics over a wide spectrum of input parameters, Fig. 6(c) depicts the transmittance ratio for forward and backward actuations with both configurations A and B as input frequency and amplitude varies. The transmittance ratio heat map shown in Fig. 6(c) is in log scale with the lighter color region corresponding to larger TR values. As demonstrated in Fig. 6(c), for both configurations A and B, wave propagation characteristics for forward and backward actuations are considerably different for various combinations of input parameters. In fact, with the given system parameters, most of the signal transmits through the chain for backward actuation, whereas for forward actuation, wave energy does not propagate for some combinations of input frequency and amplitude in the parameter space, indicated by a greater area of dark space in Fig. 6(c). Such discrepancy in TR for two excitation directions creates a region in parameter space in which nonreciprocal energy transmission exits. Additionally, this phenomenon is observed for most of the frequencies inside the stopbands. More intriguingly, as configurations switch from A to B, significant adaptation of wave propagation characteristics can be observed for forward actuations, Fig. 6(c). For instance, with input level $\delta = 1$ and frequency $\omega = 1.5$, initially blocked wave energy for configuration A can propagate through the chain as switched to configuration B. It is also worth noting that the nonpropagating zone for configuration B, indicated by the dark blue area, is much smaller compared to that for configuration A, corroborating with the previously discussed fact that configuration B corresponds to a softer state. From these observations, we can conclude that the proposed metastable metastructure is invested with massive adaptivity of nonreciprocal wave propagation characteristics for a wide frequency range by switching among the metastable states.

V. CONCLUSION

In this paper, we present an approach to achieve the on-demand adaptation of band structures and nonreciprocal wave propagation. We found that due to the inherent spatial asymmetry of the metastructure, the proposed nonlinear chain is able to trigger the onset of supratransmission at different excitation levels for forward and backward excitation scenarios, creating a region in parameter space in which unidirectional wave propagation can be realized. Additionally, exploiting the programmable properties facilitated via reconfiguring among the numerous modules and corresponding metastable states, the proposed metastructure exhibits unprecedented broadband nonreciprocal wave propagation and adaptation. By intelligently leveraging nonlinearity, spatial asymmetry, periodicity, and metastability, we demonstrated through both experiment and analysis that one can tune and control nonreciprocal wave propagation via the proposed metastable modular metastructure. Results of the present work will pave the way for further analytical, numerical, and experimental studies of adaptive nonreciprocal wave propagation in higher-dimensional systems. Last, since the approach depends primarily on scale-independent principles, it could foster a new generation of reconfigurable structural and material systems with unconventional wave characteristics that are applicable to vastly different length scales for a wide spectrum of applications.

ACKNOWLEDGMENTS

The authors gratefully acknowledge the support of the U.S. Army Research Office under Grant No. W911NF-15-1-0114. Y.Z. also acknowledges the support from China Scholarship Council.

[1] J. W. Strutt, Some general theorems relating to vibrations, Proc. London Math. Soc. **s1–4**, 357 (1871).

[2] H. Lamb, On reciprocal theorems in dynamics, Proc. London Math. Soc. **s1–19**, 144 (1887).

[3] B. Li, L. Wang, and G. Casati, Thermal Diode: Rectification of Heat Flux, Phys. Rev. Lett. **93**, 184301 (2004).

[4] B. Hu, L. Yang, and Y. Zhang, Asymmetric Heat Conduction in Nonlinear Lattices, Phys. Rev. Lett. **97**, 124302 (2006).

[5] W. Kobayashi, Y. Teraoka, and I. Terasaki, An oxide thermal rectifier, Appl. Phys. Lett. **95**, 171905 (2009).

[6] M. Maldovan, Sound and heat revolutions in phononics, Nature **503**, 209 (2013).

[7] B. Liang, X. S. Guo, J. Tu, D. Zhang, and J. C. Cheng, An acoustic rectifier, Nat. Mater. **9**, 989 (2010).

[8] M. Tocci, M. Bloemer, M. Scalora, J. P. Dowling, and C. M. Bowden, Thin-film nonlinear optical diode, Appl. Phys. Lett. **66**, 2324 (1995).

[9] J. Y. Chin, T. Steinle, T. Wehlus, D. Dregely, T. Weiss, V. I. Belotelov, B. Stritzker, and H. Giessen, Nonreciprocal plasmonics enables giant enhancement of thin-film Faraday rotation, Nat. Commun. **4**, 1599 (2013).

[10] C. W. J. Beenakker, Random-matrix theory of quantum transport, Rev. Mod. Phys. **69**, 731 (1997).

[11] A. A. Maznev, A. G. Every, and O. B. Wright, Reciprocity in reflection and transmission: What is a "phonon diode?" Wave Motion **50**, 776 (2013).

[12] R. Fleury, D. L. Sounas, C. F. Sieck, M. R. Haberman, and A. Alù, Sound isolation and giant linear nonreciprocity in a compact acoustic circulator, Science **343**, 516 (2014).

[13] N. Swinteck, S. Matsuo, K. Runge, J. O. Vasseur, P. Lucas, and P. A. Deymier, Bulk elastic waves with unidirectional backscattering-immune topological states in a time-dependent superlattice, J. Appl. Phys. **118**, 063103 (2015).

[14] D.-W. Wang, H.-T. Zhou, M.-J. Guo, J.-X. Zhang, J. Evers, and S.-Y. Zhu, Optical Diode Made from a Moving Photonic Crystal, Phys. Rev. Lett. **110**, 093901 (2013).

[15] B. I. Popa and S. A. Cummer, Non-reciprocal and highly nonlinear active acoustic metamaterials, Nat. Commun. **5**, 3398 (2014).

[16] N. Nadkarni, A. F. Arrieta, C. Chong, D. M. Kochmann, and C. Daraio, Unidirectional Transition Waves in Bistable Lattices, Phys. Rev. Lett. **116**, 244501 (2016).

[17] N. Nadkarni, C. Daraio, and D. M. Kochmann, Dynamics of periodic mechanical structures containing bistable elastic elements: From elastic to solitary wave propagation, Phys. Rev. E **90**, 023204 (2014).

[18] R. L. Harne and K. W. Wang, *Harnessing Bistable Structural Dynamics: For Vibration Control, Energy Harvesting, and Sensing* (John Wiley and Sons, New York, 2017).

[19] R. Fleury, D. Sounas, M. R. Haberman, and A. Alù, Nonreciprocal acoustics, Acoust. Today **11**, 14 (2015).

[20] S. A. Cummer, J. Christensen, and A. Alù, Controlling sound with acoustic metamaterials, Nat. Rev. Mater. **1**, 16001 (2016).

[21] N. Boechler, G. Theocharis, and C. Daraio, Bifurcation-based acoustic switching and rectification, Nat. Mater. **10**, 665 (2011).

[22] Z.-G. Chen and Y. Wu, Tunable Topological Phononic Crystals, Phys. Rev. Appl. **5**, 054021 (2016).

[23] J. R. Raney, N. Nadkarni, C. Daraio, D. M. Kochmann, J. A. Lewis, and K. Bertoldi, Stable propagation of mechanical signals in soft media using stored elastic energy, Proc. Natl. Acad. Sci. U.S.A. **113**, 9722 (2016).

[24] Z. Wu, R. L. Harne, and K. W. Wang, Exploring a modular adaptive metastructure concept inspired by muscle's cross-bridge, J. Intell. Mater. Syst. Struct. **27**, 1189 (2016).

[25] R. L. Harne, Z. Wu, and K. W. Wang, Designing and harnessing the metastable states of a modular metastructure for programmable mechanical properties adaptation, J. Mech. Des. **138**, 021402 (2015).

[26] M. Caruel, J. M. Allain, and L. Truskinovsky, Mechanics of collective unfolding, J. Mech. Phys. Solids **76**, 237 (2015).

[27] M. Caruel, J.-M. Allain, and L. Truskinovsky, Muscle as a Metamaterial Operating Near a Critical Point, Phys. Rev. Lett. **110**, 248103 (2013).

[28] M. J. Frazier and D. M. Kochmann, Band gap transmission in periodic bistable mechanical systems, J. Sound Vib. **388**, 315 (2017).

[29] B. Yousefzadeh and A. S. Phani, Energy transmission in finite dissipative nonlinear periodic structures from excitation within a stop band, J. Sound Vib. **354**, 180 (2015).

[30] F. Geniet and J. Leon, Energy Transmission in the Forbidden Band Gap of a Nonlinear Chain, Phys. Rev. Lett. **89**, 134102 (2002).

[31] R. Khomeriki, S. Lepri, and S. Ruffo, Nonlinear supratransmission and bistability in the Fermi-Pasta-Ulam model, Phys. Rev. E **70**, 066626 (2004).

[32] S. B. Yamgoué, S. Morfu, and P. Marquié, Noise effects on gap wave propagation in a nonlinear discrete *LC* transmission line, Phys. Rev. E **75**, 036211 (2007).

[33] J. Lydon, G. Theocharis, and C. Daraio, Nonlinear resonances and energy transfer in finite granular chains, Phys. Rev. E **91**, 023208 (2015).

[34] X. Fang, J. Wen, J. Yin, D. Yu, and Y. Xiao, Broadband and tunable one-dimensional strongly nonlinear acoustic metamaterials: Theoretical study, Phys. Rev. E **94**, 052206 (2016).